Surface Science 603 (2009) 419–424

Contents lists available at ScienceDirect

Surface Science

journal homepage: www.elsevier.com/locate/susc

Growth mode and novel structure of ultra-thin KCl layers on the Si(100)-2 × 1 surface

S.-F. Tsay [a], J.Y. Chung [b,c], M.-F. Hsieh [b,c], S.-S. Ferng [b,c], C.-T. Lou [b,c], D.-S. Lin [b,c,*]

[a] Department of Physics, National Sun Yat-sen University, 70 Lienhai Road, Kaohsiung 80424, Taiwan
[b] Department of Physics, National Tsing Hua University, 101 Sec. 2, Kuang-Fu Road, Hsinchu 30013, Taiwan
[c] Institute of Physics, National Chiao-Tung University, 1001 Ta-Hsueh Road, Hsinchu 30010, Taiwan

ARTICLE INFO

Article history:
Received 25 August 2008
Accepted for publication 9 December 2008
Available online 24 December 2008

Keywords:
Alkali halides
Silicon vgermanium
Scanning tunneling microscopy
Synchrotron radiation photoelectron spectroscopy
Epitaxy
Surface relaxation and reconstruction
Thin film structures
Semiconductor – insulator interfaces

ABSTRACT

This study investigates ultra-thin potassium chloride (KCl) films on the Si(100)-2 × 1 surfaces at near room temperature. The atomic structure and growth mode of this ionic solid film on the covalent bonded semiconductor surface is examined by synchrotron radiation core level photoemission, scanning tunneling microscopy and *ab initio* calculations. The Si 2*p*, K 3*p* and Cl 2*p* core level spectra together indicate that adsorbed KCl molecules at submonolayer coverage partially dissociate and that KCl overlayers above one monolayer (ML) have similar features in the valance band density of states as those of the bulk KCl crystal. STM results reveal a novel c(4 × 4) structure at 1 ML coverage. *Ab initio* calculations show that a model that comprises a periodic pyramidal geometry is consistent with experimental results.

1. Introduction

Heteroepitaxy is frequently used to develop new synthetic materials – especially semiconductors – for fundamental research and novel devices. Heterostructures that combine very dissimilar materials, such as pure ionic compounds on pure covalent crystals [1,2], have generated much interest recently owing to the realization of a variety of possible novel properties. Ionic crystals and covalent crystals are held together by attractive forces of very different nature. Understanding the growth mechanism of thin ionic crystals on covalently bonded group IV semiconductors and their interfacial property can broaden our knowledge of principles that govern heteroepitaxy and surface science.

NaCl/Ge(100) is a prototypical system for the heteroepitaxy of small-lattice mismatch ionic crystals/covalent crystal. The second nearest–neighbor separation R_1 for an NaCl crystal is 3.98 Å. The surface lattice constant *a*, or the period of unreconstructed Ge(100)-1 × 1, is 4.00 Å. The lattice mismatch at the heterostructure of NaCl/Ge(100) is close to 0.5%. Previous studies have established that NaCl can grow epitaxially on Ge(100) with a high degree of quality under suitable conditions [1,3–5]. An STM measurement suggests that the growth of NaCl begins with a carpet-like double-layer NaCl film [1]. In an electron energy loss scattering (EELS) measurement Zielasek, Hildebrandt and Henzler found electronic states at the NaCl/Ge interface and suggested that the dimerization of the Ge(100) surface is not eliminated at the NaCl/interface – even if the thickness of NaCl rises to 20 ML [2].

For large lattice mismatch systems, the growth of alkali halide on the Si and Ge surfaces at around one monolayer coverage does not yield an ordered surface structure. For example, sub-monolayer LiBr (R_1 = 3.89 Å) and LiF (R_1 = 2.85 Å) are adsorbed randomly onto Si(100) (*a* = 3.84 Å) at room temperature [6,7]. Guo and Souda observed that KI (nearest–neighbor separation R_0 = 3.53 Å) dissociatively adsorbs on the Si(100) surface at a coverage of less than 0.5 ML [8]. Although thick flat films can be obtained, the growth of KI, LiF and LiBr on Si(100) and Si(111) surfaces proceeds by the Volmer–Weber (VW) mechanism of island growth as a result of the interfacial lattice mismatch.

Potassium chloride (KCl) has the sodium chloride structure with R_1 = 4.32 Å. The heterostructure of KCl/Si(100) has a very large (13%) lattice mismatch. This study establishes that a single monolayer of KCl forms ordered superstructure on the Si(100) surface and the KCl film can be grown epitaxially. Based on *ab initio* calculations, this study demonstrates that regular arrays of four-facet pyramid-like wrinkles reduce the excess energy associated with a

* Corresponding author. Address: Department of Physics, National Tsing Hua University, 101 Sec. 2, Kuang-Fu Road, Hsinchu 30013, Taiwan. Tel.: +886 3 5742977; fax: +886 3 5723052.
E-mail address: dslin@phys.nthu.edu.tw (D.-S. Lin).

0039-6028/$ - see front matter © 2009 Elsevier B.V. All rights reserved.
doi:10.1016/j.susc.2008.12.010

large lattice mismatch. In addition to its uniqueness, this new superstructure also demonstrates the interaction between a pure ionic monolayer and the surface of pure covalent crystals.

2. Experiment

The Si(100) samples were antimony doped with a resistance of 0.01 Ω cm. After thorough outgassing at ~900 K, a dimerized clean Si(100) surface was obtained by a few seconds of heating to ~1450 K. 99.99% pure KCl was sublimated from an alumina crucible by a feedback-controlled electron bombardment beam. To minimize contamination at submonolayer coverage, the photoemission was measured immediately after KCl was deposited on clean surfaces. Above one monolayer, the deposition was often performed additively. The deposition rate was determined using an integral flux monitor that was calibrated by a quartz-crystal thickness monitor. The coverage of KCl adsorbate in ML (denoted by θ), was estimated from the exposure time, assuming the sticking coefficient is 1. The ML is referred to the surface density of the unreconstructed Si(100) surface, i.e. 1 ML = $6.8 \times 10^{14}/cm^2$. The substrate temperature during growth was approximately 330 K.

The photoemission spectra were recorded at the Taiwan Light Source laboratory in Hsinchu, Taiwan. Synchrotron radiation from a 1.5 GeV storage ring was dispersed by a wide-range spherical grating monochromator (SGM). The photocurrent from a gold mesh placed in the synchrotron beam path was monitored to determine the relative incident photon beam flux. Photoelectrons were collected from 60° off normal emission and analyzed by a 125 mm hemispherical analyzer in a μ-metal-shielded UHV system with a based pressure of $\sim 3 \times 10^{-10}$ torr. The overall energy resolution was better than 120 meV. The STM measurement was taken in a separated UHV chamber with a base pressure of 8×10^{-11} torr. The tunneling current was about 0.1 nA. The topographic height measurement did not strongly depend on the sample bias around −2.4 V typically used.

3. Results and discussion

3.1. Photoemission results

High-resolution core level photoemission spectroscopy can be performed to distinguish between atoms at nonequivalent sites and in different chemical bonding configurations, based on shifts in their binding energy [9]. Identical Voigt line shapes that consist of spin-orbit split doublets individually were used to decompose each of the Si and Cl 2*p* core level spectra into overlapping components [10]. All fitting was performed using the least-squares method. The solid curves represent the fitting results that overlap the data points. Fig. 1a and b present the respective surface-sensitive Si 2*p* and Cl 2*p* core level spectra (dots) of the Si(100) covered with various amounts of KCl. Spectra of the chlorine terminated Si(100)-2 × 1 (Cl/Si(100)) surface are also presented for reference. The Cl 2*p* spectrum for Cl/Si(100) (Fig. 1b, bottom) can be analyzed in terms of only a single component that has a pair of split doublets separated by 1.60 eV, implying that all Cl has the same Si–Cl monochloride bonding configuration [11,12]. The corresponding Si 2*p* core level spectrum (Fig. 1a, bottom) has two components, B and Si^+, that are separated by 0.90 eV. The B component was responsible for the emission from the bulk and the Si^+ component from the surface Si–Cl species [9,13].

Before KCl deposition, the Si 2*p* spectrum (Fig. 1a, second from bottom) has a prominent peak S at the lower (−0.52 eV) binding energy side and a visually indiscernible peak S' at the higher (+0.26 eV) binding energy side. These two components are attributed to emissions from the up atoms of asymmetric dimers and

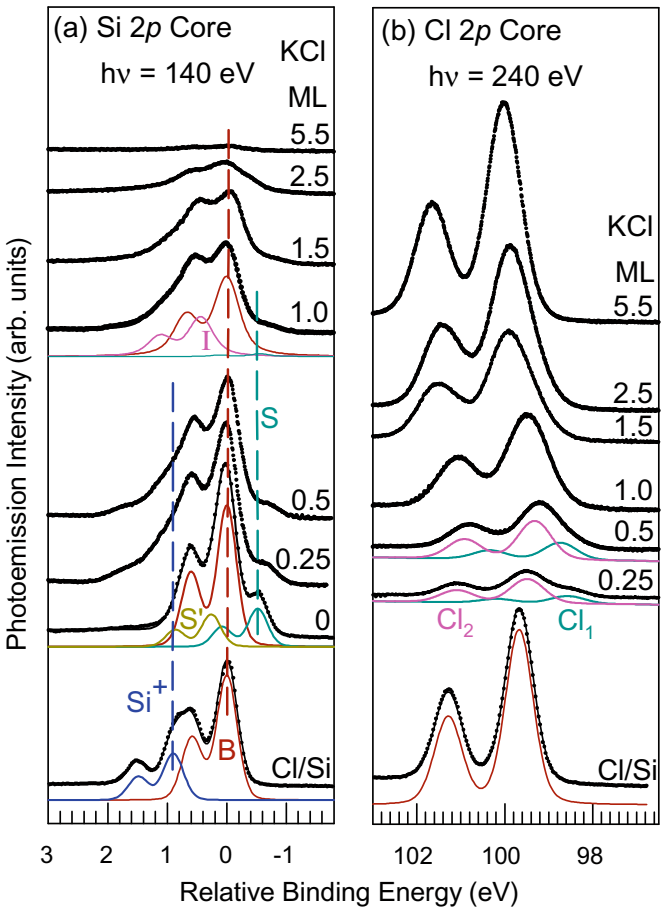

Fig. 1. (a) Si 2*p* and (b) Cl 2*p* core level photoemission spectra (circles) of Cl–Si(100)-2 × 1 surface and Si(100) surface with various amounts of deposited KCl, as labeled. The solid curves are fits to the spectra. The curves labeled B, S, I and Si^+ are the results of decomposition of the Si 2*p* spectra into contributions from the bulk, the clean surface, the interface layer and the Si–Cl species, respectively. The Cl 2*p* spectra at sub-monolayer coverage have two components Cl_1 and Cl_2. The energy zero in (a) refers to the $2p_{3/2}$ bulk position. To eliminate the band bending effect, the relative binding energy for the Cl 2*p* refers to the corresponding Si $2p_{3/2}$ line of the B component in (a). Dashed lines through the B, S, and Si^+ components are guides for the eye. (For interpretation of the references to colour in this figure legend, the reader is referred to the web version of this article.)

atoms in the second layer, respectively [14]. According to Fig. 1a and b, the integrated intensities of Cl 2*p* peak (Fig. 2) increase monotonically with the amount of KCl deposited on Si(100) at the expense of that of the Si 2*p* peak. At 5.5 ML coverage, the Si 2*p* peak is mostly attenuated, implying that KCl grows two-dimensionally.

At submonolayer coverage of KCl, the intensity of the S component in the Si 2*p* spectra declines during growth. As mentioned earlier, the S component corresponds to the negatively-charged up atoms in the dimerized layer. If the dimerized layer persists under the KCl overlayers as the atomic model suggests in Section 3.3, the disappearance of the S component suggests a reduced charge transfer between the up- and down-atoms in a dimer. Tails on the higher binding energy side for Si 2*p* with θ = 0.25 and 0.5 ML can be located near the position of the Si^+ component. Also the corresponding Cl 2*p* spectrum appears to consist of two components Cl_1 and Cl_2. These signatures together suggest that a portion of deposited KCl molecules decomposes and Si–Cl bonds are presented on the surface. The KI/Si(100) system exhibited similar decomposition of adsorbed alkali halide. Cl_2 has a larger intensity and its binding energy is close to that of thicker films. It is likely

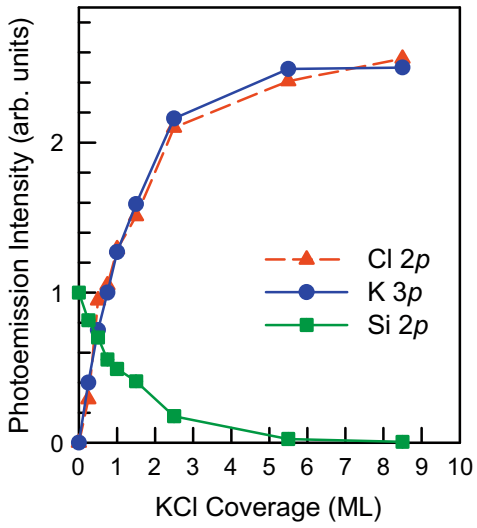

Fig. 2. Integrated photoemission intensities of Si 2*p*, Cl 2*p* and K 3*p* as functions of KCl coverage. Data for Cl 2*p* and K 3*p* are normalized to the intensity measured at KCl coverage of 1 ML. Si 2*p* is normalized to the clean surface before KCl deposition.

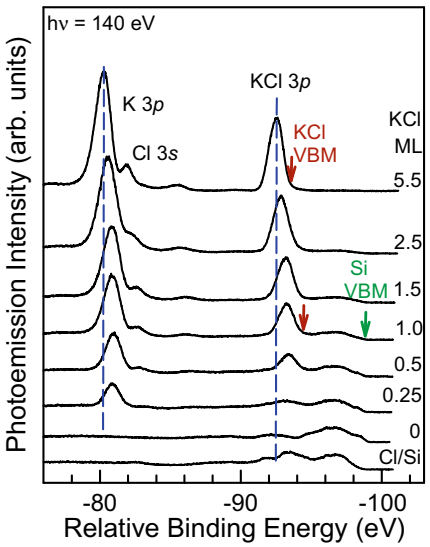

Fig. 3. Valence band region of Si(100) surface with various KCl coverage, as indicated. As in Fig. 1(b), the relative binding energy refers to the corresponding Si $2p_{3/2}$ line of the B component in Fig. 1(a). Vertical dashed lines are a guide to the eye to show the general trend in the binding energy shifts of K 2*p* and Cl 3*p*.

that Cl_2 is responsible for emission from KCl clusters (as discussed in Section 3.2). Assuming that Cl_2 corresponds Cl from decomposed KCl, its lower binding energy position may originate from the effect of nearby adsorbed K. The Si 2*p* spectrum for $\theta = 1.0$ is broad and can be described by an additional second component (denoted as *I*) on the higher binding energy side of B. The intensity ratio of *I* and *B* ($I/B = 0.49$) is about twice that of S and *B* for Si(100). Since S is responsible for $\frac{1}{2}$-ML up atoms, the atomic population for *I* is about 1.0 ML. Thus, we believe that component *I* corresponds to emission from the top Si layer under the KCl film.

Fig. 3 presents corresponding photoemission spectra in the valence band region of the same Si(100) surface with various KCl coverage. Fig. 2 plots the integrated intensities of the K 3*p* peaks, *i.e.* indicative of surface potassium population. The potassium population similarly increases with the amount of KCl deposited. The peak labeled KCl 3*p* is present above 0.25 ML, indicating that the peak is characteristic of ionic KCl clusters or films. At high coverage, the photoemission spectra are similar to those of thick KCl films [5]. During growth, the valence band emission (Cl 3*p*) from the KCl films slowly dominates while that from the Si(100) substrate is attenuated. According to Fig. 3, features of the KCl valence band begin to develop between 0.25 and 0.5 ML. As discussed above, this finding correlates with the decomposition of KCl at low coverage. When $\theta = 1.0$ ML, the silicon valence band remains detectable and the valence band offset (ΔE_v) of −4.4 eV is directly determined from the difference between the onsets of Si and KCl valence band photoemission (VBM). Although Si VBM varies only slightly, KCl VBM shifts substantially downwards. ΔE_v gradually decreases to −5.2 eV at 5.5 ML. The trend in the VBM shift resembles that of the LiF/Ge(100) system [15].

3.2. STM results

The clean double-domain Si(100) surface comprises rows of dimers [16]. Figs. 4 and 5 present the evolution of the Si(100) surface following KCl deposition at 330 K. In Fig. 4 white arrows indicate the dimer-row directions in the top Si layer before deposition. When a small amount of KCl is adsorbed, noisy images produced by the unstable feedback loop are commonly observed. Apart from a few dark sites on the dimerized surface as shown in the clearer images, such as that in Fig. 4a, no distinctive KCl adsorption species

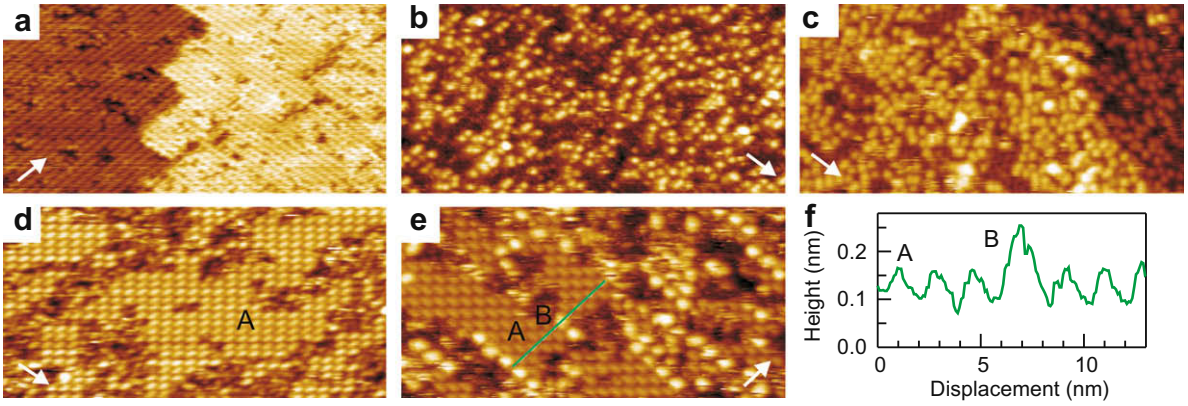

Fig. 4. STM images of coverage evolution with deposition of (a) 0.1, (b) 0.3, (c) 0.5, (d) 0.8 and (e) 1.2 ML KCl on Si(100)-2 × 1 surface. The sample bias was −2.4 V. The images cover an area of about 40 × 20 nm^2. The white arrows indicate the dimer-row direction in the top silicon layer. (f) Apparent topographic height profile along the green line in (e) from lower-left to upper-right. B: position of one Cluster B. (For interpretation of the references to colour in this figure legend, the reader is referred to the web version of this article.)

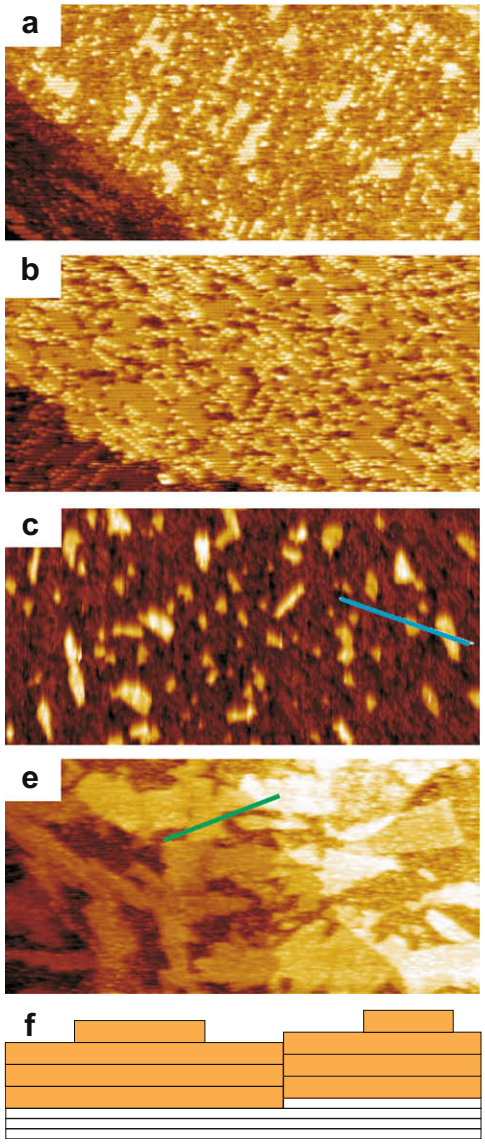

Fig. 5. Large-area STM images of coverage evolution with deposition of (a) 0.6, (b) 1.2, (c) 2.4 and (d) 3.6 ML KCl on the Si(100)-2 × 1 surface. The sample bias was −2.4 V. In (d), two substrate steps (0.14 nm in height) in the lower-left and upper-right corners remain discernible. (e) Schematic showing KCl films (orange) of several layers thick has a bulk-like structure on Si(100). Two atomic steps with heights of 0.315 and 0.14 nm show the interlayer spacings for KCl(100) and Si(100), respectively. (a), (b) and (c) cover an area of 200 × 100 nm^2 and (d) covers an area of 300 × 150 nm^2. (For interpretation of the references to colour in this figure legend, the reader is referred to the web version of this article.)

or cluster is observed at $\theta < 0.2$ ML. The dark sites have a similar appearance to those found in Cl adsorption on Si(100) [12]. The unstable scans and fewer-than-expected apparent absorption species together indicate that the deposited KCl molecules at low coverage, if not decomposed, are not strongly chemisorbed and are probably quite mobile on the clean Si surface. This finding agrees with the results of photoemission described earlier. As discussed in the preceding section, the valence band and core level spectra show no KCl characteristics until above 0.25 ML and that some of the adsorbed KCl molecules decompose. The dissociated Cl atoms easily generate Si–Cl bonds, which are likely responsible for the many dark sites in the image other than the original defects on the surface.

As KCl adsorption accumulates above 0.3 ML, many random bright protrusions develop and grow, as presented in Fig. 4b and c. Between these protrusions, the dimer rows remain clearly visible. At 0.5 ML, these protrusions have a more uniform size than at 0.3 ML and their apparent height is determined to be 1.6 Å. Their absence below 0.2 ML and their areal size suggest that these protrusions are probably nucleated clusters of KCl that are formed following critical super saturation of mobile KCl surface species [17]. Above 0.6 ML, well-ordered c(4 × 4) arrays of protrusions appear and grow in size amid the disordered clusters, as displayed in Figs. 5a and 4d. Each c(4 × 4) cell has a single elongated elliptical protrusion, whose semi-major axis is perpendicular to the row of dimers in the substrate. Although the atomic features are not resolved, the size of these protrusions suggests that each protrusion is a KCl cluster. Such clusters are denoted Clusters A. At 1.0 ML the c(4 × 4) domains expand to fill the terraces (Fig. 5b). According to Fig. 4d and e, the c(4 × 4) areas are separated by domain boundaries with no apparent atomic ordering. At a coverage of over 1 ML, new clusters (Cluster B) appear as even brighter protrusions than Clusters A in Figs. 4e and 5b. The STM measurement does not resolve details of the atomic structure of Clusters B. Clusters B randomly disperse in the area of c(4 × 4) domain boundaries and often form linear chains. Fig. 4f presents the line profile across Clusters A and B. The plot shows that the typical apparent corrugation in the c(4 × 4) regions is around 0.7 Å. The apparent height difference between Clusters A and B is approximately 1.0 Å.

The STM image such as that in Fig. 5c reveals that two dimensional islands emerge and grow as KCl grow above 2 ML. The carpet-like growth that is observed in the NaCl/Ge(100) system is not observed here. The apparent height of these islands (Fig. 6a)extracted from line scans is about 2.2 Å above Clusters B, which cover much of the surface. The apparent height of these islands above the top silicon layer is thus estimated to be about 4.8 Å. This measurement notably exceeds the value of 3.15 Å, which is expected for a single KCl monolayer, but is less than that for a double-layer. A previous study indicated that the increase in the effective tunneling barrier over the insulating thin films leads to the underestimation of the apparent height [1]. Another study demonstrated that the growth of a second alkali halide monolayer flattens the corrugated first monolayer on a similar covalent bonded Ge(100) surface [18]. Above observations indicate that these flat-top islands are either KCl double layers or triple layers.

Fig. 5d presents the surface morphology after 3.6 ML of KCl deposition. The main features in the image are large-area islands on flat terraces or on even larger islands. The step height (Fig. 6b) of these islands measures about 3.0 Å, *i.e.* close to the height of a single KCl monolayer. The step structure with steps of

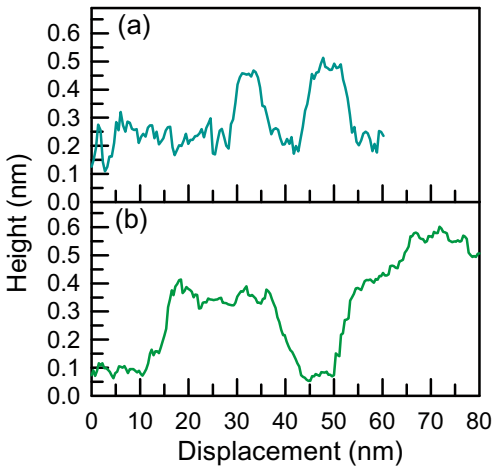

Fig. 6. Apparent topographic height profiles (a) and (b) (from left) along lines marked in Fig. 5c and d, respectively.

alternative types A and B found in the clean Si(100) before KCl deposition remains clearly discernible in the large area image. Again, islands do not extend across the monoatomic steps because of the mismatch between the lattice spacings of the Si(100) substrate and the KCl films. These findings indicate that further KCl deposition above 2 ML follows pseudo layer-by-layer growth and that KCl films with a thickness of more than two (or three) layers no longer have a commensurate KCl/Si(100) interface as schematically shown in Fig. 5e. In heteroepitaxy small lateral lattice mismatches generally produce layer-by-layer growth while large mismatches result in three-dimensional growth. Local-density approximation (LDA) calculations have demonstrated that the adsorption energy of the first NaCl layer on the Ge(100) surface is 0.2654 eV/(1 × 1) unit cell [18]. The adsorption energy increases to 0.3844 eV and 0.4069 eV per unit cell for the second and third layer, respectively, because of the presence of more bulk-like ionic solids and reduction in the non-planar arranged cations and anions in the first layer. The adsorption energy of the first NaCl layer on Ge(100) is compatible to that found on Ag(100) [19]. These considerations support our postulation that thick KCl films on Si(100) have a structure similar to the bulk crystal. Therefore, the KCl growth proceeds in a layer-by layer fashion as in alkali halide/metal systems.

3.3. Atomic model of c(4 × 4) surface structure

As described in Section 3.3, the c(4 × 4) domains cover most of the surface at 1 ML KCl coverage. The STM image, such as that in Fig. 7a, shows only one protrusion in one c(4 × 4) unit cell. Details on the atomic scale are not resolved. To determine the atomic structure of the grown KCl layer, we used the Vienna *ab initio* Simulation Package (VASP) code within density-functional theory of LDA. The Ceperley-Alder exchange-correlation function, as parameterized by Perdew and Zunger, was adopted. Following the standard procedure [20–22], a 4 × 4 repeated-slab supercell model was adopted. Each slab has ten atomic layers of Si and the adlayers of K and Cl; H atoms are bound to the bottom-layer Si atoms to saturate their dangling bonds. The heights of the supercell in the [001] direction were fixed at 6 nm, which sufficed to prevent coupling between the slabs. By fixing the bottom double Si and H layers, the structure was optimized until the residual force acting on each atom was less than 0.01 eV/Å.

Fig. 7b, c and d present the top view, the perspective view and the projections of ion positions of the relaxed structure for 1 ML KCl/Si(100), obtained by VASP calculations. Fig. 7b indicates that the projection of Cl ions on the (100) plane remains roughly a two-dimensional square lattice. A sodium cation is located near the center of each square of anions. This arrangement of ions of alternating charge reduces the Madelung energy, as in all ionic crystals. However, the second nearest–neighboring (Cl–Cl) separation of KCl crystal is 4.32 Å, almost 13% greater than the lattice constant (3.83 Å) of the unreconstructed Si(100) surface. Fig. 7c and d show that the ions increase their separations by forming four micro-facets, or a square pyramid-like shape, to reduce the excess energy associated with overlapping in atomic orbits. The angle of inclination of the pyramid is about 33°, yielding a nearest-neighboring K–Cl separation that is similar to that of a KCl crystal. The alternative layer structure of the pyramidal-arranged cations and

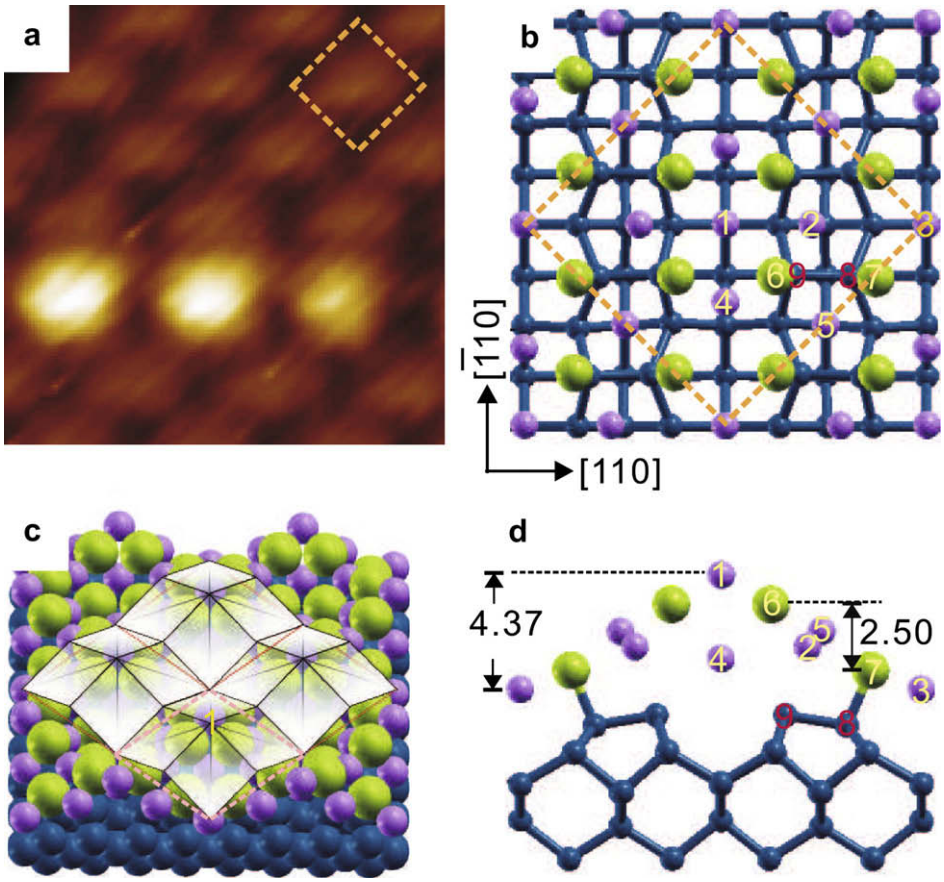

Fig. 7. (a) Close-up image of c(4 × 4) structure extracted from Fig. 5b. Pink dashed rectangle denotes unit cell of ordered Cluster A. Bright protrusions on lower area are Cluster B. (b) Top view, (c) perspective view, and (d) (1̄,1,0) projection of atomic model of c(4 × 4) structures. Blue, green and purple circles represent Si, Cl and Na atoms, respectively. (For interpretation of the references to colour in this figure legend, the reader is referred to the web version of this article.)

anions also helps to reduce the flat-lying dipoles. Structural details and its electronic properties of this c(4 × 4) model can be found elsewhere [23].

3.4. Conclusion

The growth and morphology of KCl thin films deposited on a Si(100) surface at 330 K in the coverage range of 0–5.5 ML were observed by combined photoemission spectroscopy and scanning tunneling microscopy (STM). At low coverage, some KCl molecules dissociate. Above 0.3 ML, adsorbed KCl precipitates in clusters. At about 1 ML coverage, most surface area is covered by regular clusters (Cluster A) that produce a c(4 × 4) ordered surface structure. *Ab initio* calculations support a novel four-sided pyramidal model for the first KCl monolayer. Between 1 and 2 ML, further adsorbed KCl coalesces into regular clusters of the second kind (Cluster B). The atomic structure of Clusters B was not resolved. Above 2 ML, pseudo-two-dimensional growth occurs, while the monoatomic steps on the Si(100) substrate advance through the growing films.

Acknowledgements

This work is supported by the National Science Council of Taiwan under Contract No. NSC 95-2112-M009-0039-MY4 (DSL) and NSC 95-2112-M-110-016 -MY3 (SFT) and by the National Synchrotron Radiation Research Center and National Center for High-Performance Computing at Hsinchu, Taiwan.

References

[1] K. Glöckler, M. Sokolowski, A. Soukopp, E. Umbach, Phys. Rev. B 54 (1996) 7705.
[2] V. Zielasek, T. Hildebrandt, M. Henzler, Phys. Rev. B 69 (2004) 205313.
[3] C. Schwennicke, J. Schimmelpfennig, H. Pfnür, Surf. Sci. 293 (1993) 57.
[4] S. Folsch, U. Barjenbruch, M. Henzler, Thin Solid Films 172 (1989) 123.
[5] G.K. Wertheim, J.E. Rowe, D.N.E. Buchanan, P.H. Citrin, Phys. Rev. B 51 (1995) 13675.
[6] M. Katayama, K. Ueno, A. Koma, M. Kiguchi, K. Saiki, Jpn. J. Appl. Phys. 43 (2004) L203.
[7] H. Guo, H. Kawanowa, R. Souda, Appl. Surf. Sci. 158 (2000) 159.
[8] H. Guo, R. Souda, J. Appl. Phys. 92 (2002) 6621.
[9] F.J. Himpsel, F.R. McFeely, J.F. Morar, A. Taleb-Ibrahimi, J.A. Yarmoff, Photoemission and Adsorption Spectroscopy of Solids and Interfaces with Synchrotron Radiation, in: G. Scoles (Ed.), Proceedings of the International School of Physics "Enrico Fermi" Course CVIII, North-Holland, New York, 1991.
[10] T.-C. Chiang, CRC Crit. Rev. Solid State Mater. Sci. 14 (1988) 269.
[11] H.N. Waltenburg, J.T. Yates Jr., Chem. Rev. 95 (1995) 1589.
[12] I. Lyubinetsky, Z. Dohnalek, W.J. Choyke, J.T. Yates, Phys. Rev. B 58 (1998) 7950.
[13] D.-S. Lin, J.L. Wu, S.-Y. Pan, T.-C. Chiang, Phys. Rev. Lett. 90 (2003) 046102.
[14] E. Landemark, C.J. Karlsson, Y.-C. Chao, R.I.G. Uhrberg, Phys. Rev. Lett. 69 (1992) 1588.
[15] D.A. Lapiano-Smith, E.A. Eklund, F.J. Himpsel, L.J. Terminello, Appl. Phys. Lett. 59 (1991) 2174.
[16] J.J. Boland, Adv. Phys. 42 (1993) 129, and references therein.
[17] J.B. Hudson, Surface Science: An Introduction, Butterworth-Heinemann, Boston, 1991, p. 289.
[18] S.-F. Tsay and D.S. Lin, (2008) unpublished.
[19] M. Pivetta, F. Patthey, M. Stengel, A. Baldereschi, W.-D. Schneider, Phys. Rev. B 72 (2005) 115404.
[20] G. Kresse, J. Hafner, Phys. Rev. B 47 (1993) R558;
G. Kresse, J. Hafner, Phys. Rev. B 14251 (1994) 49.
[21] G. Kresse, J. Furthmüller, Phys. Rev. B 54 (1996) 11169.
[22] G. Kresse, J. Furthmüller, Comput. Mat. Sci. 6 (1996) 15.
[23] S.-F. Tsay, unpublished.